

Research Article

Experimental Investigation of Nonlinear Energy Evolution and Failure Characteristics of Granite under Different Water Content States

Jiaqi Guo ¹, Hengyuan Zhang ¹, Feiyue Sun,¹ Junqi Fan ² and Xiaoyan Shi²

¹College of Civil Engineering, Henan Polytechnic University, Jiaozuo, Henan 454003, China

²Institute of Defense Engineering, AMS, PLA, Luoyang, Henan 471023, China

Correspondence should be addressed to Junqi Fan; lyfq@163.com

Received 10 July 2022; Accepted 20 August 2022; Published 5 September 2022

Academic Editor: Dongjiang Pan

Copyright © 2022 Jiaqi Guo et al. This is an open access article distributed under the Creative Commons Attribution License, which permits unrestricted use, distribution, and reproduction in any medium, provided the original work is properly cited.

To study the energy evolution law and failure characteristics of granite under different water content states, a series of compression failure tests of dry, natural, and saturated granite samples under different confining pressures were carried out based on the RMT-150B rock mechanics test system. The research results show that the compressive strength, cohesion, and internal friction angle of granite samples decrease to different degrees with increased water content. The growth rate of the total input energy and elastic strain energy of granite samples in the energy evolution process decreases with increased water content. The higher the water content of granite samples, the lower the total input energy, the slower the elastic strain energy rises, the lower the energy storage limitation, the earlier the dissipation energy starts to increase rapidly, and the lower the final energy dissipated. Based on the principle of self-repression of energy, a nonlinear model and its mathematical equations for the energy evolution of granite are established. The higher the water content of granite samples, the greater the energy iterative growth factor and its increasing rate, and the lower the deviator stress level of granite sample systems entering the period-doubling bifurcation and chaos areas. The samples show three failure modes: splitting failure, splitting-shear composite failure, and shear failure. The failure modes of granite samples have an excellent matching relationship with the distribution range of its energy storage limitation. When the energy storage limitation of the samples is minor, it is more likely to occur splitting failure. When the energy storage limitation of the samples is significant, it is more likely to occur shear failure.

1. Introduction

With the steady and rapid development of China's national economy, rock mass projects in the fields of energy/resource development, transportation infrastructure, water conservancy, and hydropower have been or will be constructed in large quantities [1, 2]. The above projects are often affected by groundwater in the process of construction and operation. Water has pronounced softening, dissolving, and wedge effects on engineering rock mass. This leads to complex physical, chemical, and mechanical processes between water and rock, which have a nonnegligible impact on the strength, deformation, permeability, energy evolution, and damage characteristics of the engineering rock mass. Make the mechanical properties of the engineering rock body

show a considerable degree of the weakening phenomenon, reduce the stability of rock engineering, and cause various types of rock engineering disasters [3]. According to relevant statistics, more than 90% of the failure and instability of rock slopes and 60% of the mine accidents are related to water, and 30%~40% of the dam accidents in water conservancy and hydropower projects are caused by the action of water [4]. Since 2000, there have been more than 600 water inrush disasters in tunnels and underground projects in China, with thousands of casualties and huge economic losses resulting in severe social impacts [5]. Therefore, it is of great significance to study the influence of water on mechanical properties, energy evolution process, and failure characteristics of engineering rock mass for rock mass engineering design and engineering disaster prevention and control.

In recent years, many scholars at home and abroad have carried out fruitful research on rock mechanical properties, energy characteristics, and failure modes under different saturated conditions. Guo et al. [6] studied the influence of the saturated state on the strength, deformation, and energy characteristics of karst limestone. They considered that the real-time evolution process of energy in the whole process of karst limestone samples has apparent stages. The variation of dissipation energy difference with confining pressure is the internal reason for the difference in failure forms of samples with different water content. Tian-bin et al. [7] used the MTS815 rock mechanics test system to carry out the conventional triaxial compression tests of sandstone under five water content states. They found that the energy storage capacity and strain energy release capacity of sandstone specimens decreased with increasing water content, the energy dissipated by rock deformation failure decreased, the brittle failure characteristics of the rock weakened, and the plastic failure characteristics increased. Chen et al. [8] studied the laws of water influence on the stress-strain relationship, cracking behavior, and energy evolution of sandstone. Chen et al. [9] carried out some uniaxial and triaxial compression tests to investigate the effect of confining pressure and water content on the mechanical properties, fracture evolution, and energy damage mechanism of deep-buried carbonaceous slate under natural and saturated states. They found that the dissipation energy gradually increased at the prepeak and postpeak stages with the increase of the confining pressure and water content. Wang et al. [10] conducted the experimental analysis of the energy revolution character of the Hawkesbury sandstone specimen from Gosford quarry in Sydney, Australia, by rating loading and unloading tests. It was found that increasing water content relieved energy release and catastrophe failure of the rock specimen and weakened elastic energy storage capacity. Zhao et al. [11] collected the dry and saturated calcium argillaceous cemented sandstone specimens from Yulin Coal mining in Shaanxi Province, China, for the uniaxial and cyclic loading experiments, and the mechanical parameters and the dissipation energy characteristics of sandstone specimens with two water contents had been comparatively analyzed. Jiang et al. [12] conducted triaxial compression tests of dried, natural, and saturated mudstone samples using the RMT-301 rock mechanics test system. Research showed that the energy storage limitation of mudstone decreases with the increase of water content and the dissipation energy increases with the rise in water content. Geng and Cao [13] performed uniaxial compression tests on sandstone with variable water contents (dry, natural, and saturated). They analyzed the deformation, damage evolution, and failure process using acoustic emission and energy dissipation. Lai et al. [14] used rock mechanics test system and full-information acoustic emission information analyzer to carry out uniaxial compression tests of coal and rock samples with different water content states. The mechanical properties, energy release law, failure mode, and acoustic emission signal characteristics of critical parts of coal and rock samples under different water contents were obtained. Li et al. [15] carried out uniaxial compression, cyclic loading, and

unloading test using the RMT-150B rock mechanics test system to study the energy storage characteristics and failure morphology of white sandstone samples under different water content. Ma et al. [16] carried out a series of uniaxial compression tests to estimate the evolution of mechanical properties, energy, and failure with the change of immersion time for gypsum rock obtained from Luneng Taishan gypsum mine in Shandong Province of China.

The above research results have deepened the understanding of the laws of water influence on the mechanical properties, energy characteristics, and failure modes of rocks. These studies have enriched and promoted the development of this field. However, the current research still has more deficiencies in the nonlinear law of energy evolution of hard rock deformation process under complex conditions, water content effect of energy characteristics, nonlinear model of energy evolution and chaos characteristics analysis, energy mechanism of hard rock failure form generation, etc. Therefore, it is urgent to carry out in-depth and systematic research on the energy nonlinear evolution mechanism of granite and other hard rocks under the combined influence of water content and confining pressure and the internal energy causes of the failure modes generation. In this study, based on the current research status, a series of compression tests on granite samples under different conditions of confining pressure and water content were carried out using the RMT-150B rock mechanics test system. Analyzed the water content and enclosing pressure effects of granite strength and deformation. The nonlinear characteristics of the energy evolution during the deformation and failure of granite under different confining pressure and water content state conditions were studied. Then, the nonlinear model and mathematical equations were established for the energy evolution of granite. Through the nonlinear model, the chaotic characteristics of energy evolution are explored and revealed the failure modes of hard rocks such as granite under the combined influence of water content and confining pressure and the energy-driven mechanisms of their generation and transformation. The research results are significant for revealing the causes of rock mass engineering disasters in water-rich areas and their prediction and prevention.

2. Sample Preparation and Test Scheme

2.1. Sample Preparation. The granite samples used for the tests in this paper were taken from Wulian County, Rizhao City, Shandong Province, China, and the sampling locations are shown in Figure 1(a). The granite is off-white with black mottling and is coarse-grained granite, as shown in Figure 1(b). To avoid the influence of the difference of the rock samples on the test results, the samples used in this test were taken from the same rock plate with complete structure, and the drilling angle was consistent during sampling. Reference the International Society of Rock Mechanics (ISRM) standard [17]. The rocks were processed into cylindrical samples, each $\Phi 50\text{mm} \times 100\text{mm}$. The maximum parallelism of the two ends of the samples was not more than 0.02 mm, and the end surface

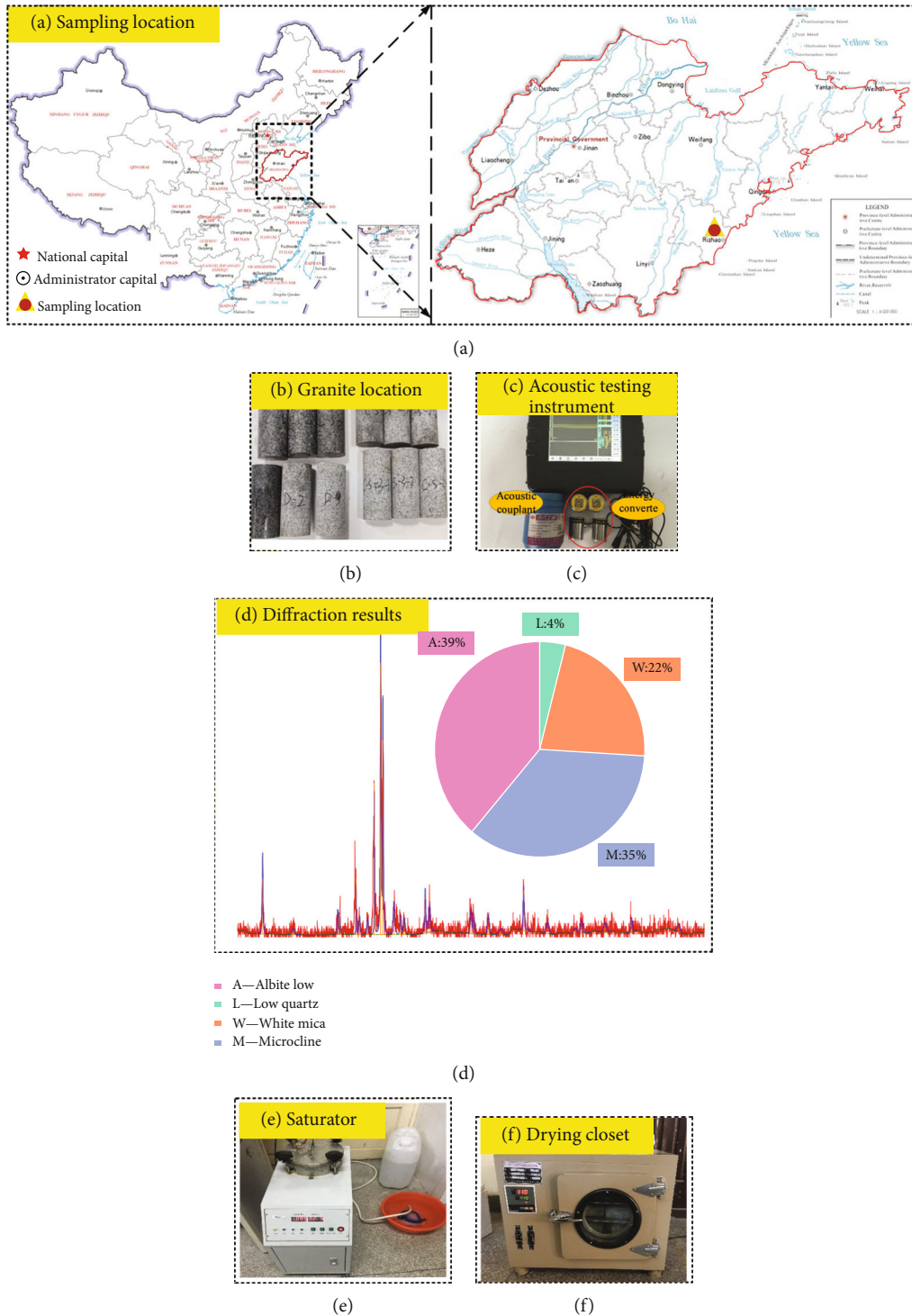


FIGURE 1: Sampling site and sample preparation for coarse-grained granite and related tests.

was perpendicular to the axis of the samples. The maximum deviation was not more than 0.2° , and the height was accurate at 1mm. After the granite samples were processed, the density and longitudinal wave velocity of all samples under natural conditions were tested (see Figure 1(c)), and the samples with a significant deviation of longitudinal wave velocity were eliminated. The average density of granite samples used in this laboratory test is

2.839 g/cm^3 , and the average longitudinal wave velocity is 5.682 km/s . The X-ray diffraction (XRD) semiquantitative analysis results of the granite samples used in the test (see Figure 1(d)) show that the rock samples are mainly composed of feldspar, mica, and quartz, among which the low albite is the most, with a content of 39%, followed by microcline feldspar, the content is about 35%, the content of muscovite is 22%, and the content of quartz is 4%.

To avoid the interference of other factors, the sampled and formed granite samples were left in the natural environment for 24 h, which are natural state samples. The author approximately believes that the moisture content of the prepared samples is the same, and the water content is 0.0919%. Dry and saturated state samples were obtained by drying and forced saturation according to the law of water absorption and dehydration (see Figures 1(e) and 1(f)). The specific process is as follows:

- (1) The dry state samples were prepared by the drying method. The granite samples were placed in the drying oven at 105°C for 24 h, and then the samples were placed in the drying container and left to room temperature. The granite samples were in a dry state with 0% water content
- (2) The saturated state samples were prepared by forced saturation. The granite samples were placed in the rock vacuum saturator, pumped to 100 kPa and left for 2 h, injected water into the vacuum saturator to submerge the samples, continued to pump to 100 kPa and kept for 1 h, and then opened the bleeder valve and left for 24 h, after which the samples were taken out and wiped off the surface water, at which time the granite samples were in the saturated state, and the average water content was tested to be 0.287%

2.2. Test Instruments and Schemes. This test adopts the RMT-150B rock mechanics test system developed by the Wuhan Institute of Geomechanics, Chinese Academy of Sciences, as shown in Figure 2.

The test system has the advantages of simple operation, good control performance, and a high degree of automation and can carry out uniaxial, triaxial whole process tests and direct shear tests. The test process can be interfered with artificially to change the test parameters (waveform, frequency, rate, control mode, limit value, etc.) to meet the needs of various special tests and theoretical research.

In this test, the uniaxial compression test (the confining pressure is 0 MPa) adopts the axial displacement control loading method. The change rate of loading displacement is set to 0.002 mm/s, and the load is applied along the axial direction until the samples are destroyed. The confining pressure levels in the conventional triaxial compression test are 5 MPa, 10 MPa, and 20 MPa, respectively. The procedure is as follows: firstly, the confining pressure is loaded at a loading rate of 0.05 MPa/s, and axial pressure is loaded simultaneously at a loading rate of 1 kN/s, when the confining pressure is loaded to the set value and kept constant, and then the axial displacement control loading mode is changed to an axial loading rate of 0.002 mm/s until a complete stress-strain curve is obtained.

3. Water Content Effect of Strength and Deformation Characteristics

3.1. Characteristic of the Whole Process Stress-Strain Curve. The uniaxial and triaxial compression tests of granite sam-

ples in dry, natural, and saturated states under different confining pressures are carried out using the RMT-150B rock mechanics test system. The whole process stress-strain curves under different conditions are obtained in Figure 3.

It can be seen from Figure 3 that the whole process stress-strain curves of granite samples in dry, natural, and saturated states under different confining pressures have apparent stages. And that can be divided into the compaction stage (OA stage), elastic stage (AB stage), plastic stage (BC stage), and failure stage (after point C). During the whole loading process, stress-strain curves of the granite sample showed a plastic-elastic-plastic S shape before the peak.

In the compaction stage (OA stage), the whole process stress-strain curve rises slowly, and the total axial strain increases with increased water content. In contrast, the total axial strain decreases with the increase of confining pressure. In the elastic stage (AB stage), the whole process stress-strain curve shows an apparent linear increase trend. The lower the water content, the higher the confining pressure, and the greater the curve slope. The elastic stage of the sample under the condition of low water content and high confining pressure is longer, and the threshold stress value of the crack initiation point is greater. The plastic stage (BC stage) of the whole process stress-strain curve of the granite sample is relatively short, and the slope of the curve gradually decreases after the elastic stage. This stage is more evident with the increase of water content and confining pressure of the sample. The peak stress of granite samples decreases with the increase of water content and increases with the growth of confining pressure. In the failure stage (after point C), the stress drop phenomenon appears after the peak of the whole stress-strain curve of the granite sample under the condition of low confining pressure and low water content, and the failure is accompanied by the ejection of debris and noticeable failure sound. The failure of the sample under the condition of high confining pressure or high water content shows ductility characteristics. With the increase in confining pressure and water content, the ductility failure characteristics of the granite sample are more pronounced.

3.2. Characteristic of the Mechanical Parameters of Samples. The compressive strength of dry, natural, and saturated granite samples under different confining pressures is shown in Figure 4(a).

As shown in Figure 4(a), water has a significant effect on the compressive strength of granite samples. Taking the confining pressure of 5 MPa as an example, the compressive strength of the sample in the dry state is 240.5 MPa, the compressive strength of the sample in the natural state is 203.1 MPa, and the compressive strength of the sample in the saturated state is 169.9 MPa. The compressive strength of the saturated and natural state samples is 70.6% and 84.4% of the dry state sample, respectively. When the confining pressure is 0 MPa, the compressive strength of the saturated and natural state samples is 66.8% and 79.5% of that of the dry state sample, respectively. When the confining pressure is 10 MPa, the compressive strength of the saturated and natural state samples is 68.0% and 85.1% of that of the

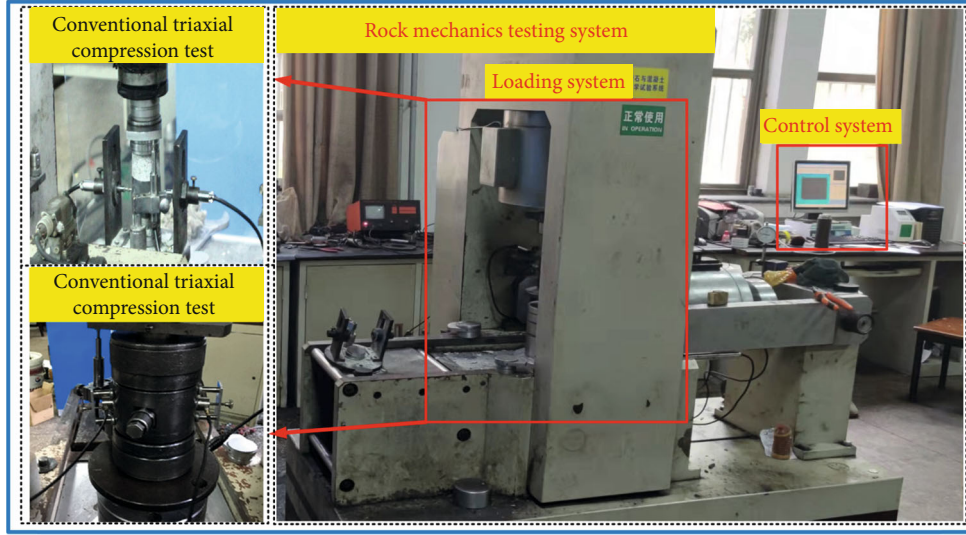


FIGURE 2: RMT-150 rock mechanics test system and test situation.

dry state sample, respectively. When the confining pressure is 20 MPa, the compressive strength of the saturated and natural state samples is 82.9% and 87.2% of that of the dry state sample, respectively. The effect of water on the compressive strength of granite samples diminished as the confining pressure increased. In the field of rock mechanics, the Mohr-Coulomb criterion is a commonly used criterion to describe the strength characteristics of rocks. The relationship of the strength criterion expressed by principal stress is as follows:

$$\sigma_1 = \xi \sigma_3 + \sigma_c, \quad (1)$$

where σ_1 is the triaxial compressive strength of the rock, σ_3 is the confining pressure, ξ is the influence coefficient of the confining pressure on the rock compressive strength, and σ_c is the theoretical uniaxial compressive strength of the rock. According to Equation (1), the compressive strength and confining pressure of granite samples with different water content states are fitted, and the fitting relationship is shown in Figure 4(b).

Figure 4(b) shows that the compressive strength of dry, natural, and saturated state samples increases with the increase of the confining pressure. The compressive strength of the samples with different water content shows an excellent linear fit with the confining pressure. The fitting relation coefficients (R^2) under three conditions are more than 0.941, indicating that the Mohr-Coulomb strength criterion can better characterize the relationship between the compressive strength and confining pressure of granite samples with different water content states. From the influence coefficient (ξ) of confining pressure on the compressive strength of granite samples in three water content states, the increase rate of compressive strength of samples in the dry state with confining pressure is greater than that in the natural state, and the increase rate in the natural state is greater than that in the saturated state. The above phenomenon reflects that the confining pressure sensitivity of the compressive strength of the sample varies with the different water content states. And

the state of water content significantly affects the confining pressure effect of the compressive strength of the sample.

In Equation (1), ξ and σ_c are strength parameters related to rock cohesion (c) and internal friction angle (φ), and their relationship with c and φ is shown as

$$\begin{aligned} \xi &= \frac{1 + \sin \varphi}{1 - \sin \varphi}, \\ \sigma_c &= \frac{2c \cos \varphi}{1 - \sin \varphi}. \end{aligned} \quad (2)$$

According to Equation (2) and the Mohr-Coulomb strength criterion fitting equation for the compressive strength of granite samples with the confining pressure, the cohesion and the internal friction angles can be calculated. Results displayed that the cohesion of dry, natural, and saturated granite samples are 32.055 MPa, 25.319 MPa, and 20.324 MPa. The internal friction angles are 54.55°, 54.39°, and 54.24°, respectively. The relationship between the cohesion, internal friction angle, and water content of granite samples with different water content states are fitted, and the fitting results are shown in Figure 5.

As depicted in Figure 5, the cohesion and internal friction angle of granite samples show nonlinear decreasing characteristics with increased water content. That is due to the water film wrapping the mineral particles, changing the shear properties between mineral particles, and softening and dissolving some debris. The cohesion of the samples decreases more significantly with the increase of water content, while the decrease of the internal friction angle is relatively small. From the dry state (0.0% water content) to the saturated state (0.287% water content), the cohesion of granite samples decreased by 36.596%, and the internal friction angle decreased by only 0.568%. The relationship between cohesion, internal friction angle, and moisture content of granite samples can be characterized by the negative exponential function based on e , and the fitting relation coefficients (R^2) are above 0.999. With the

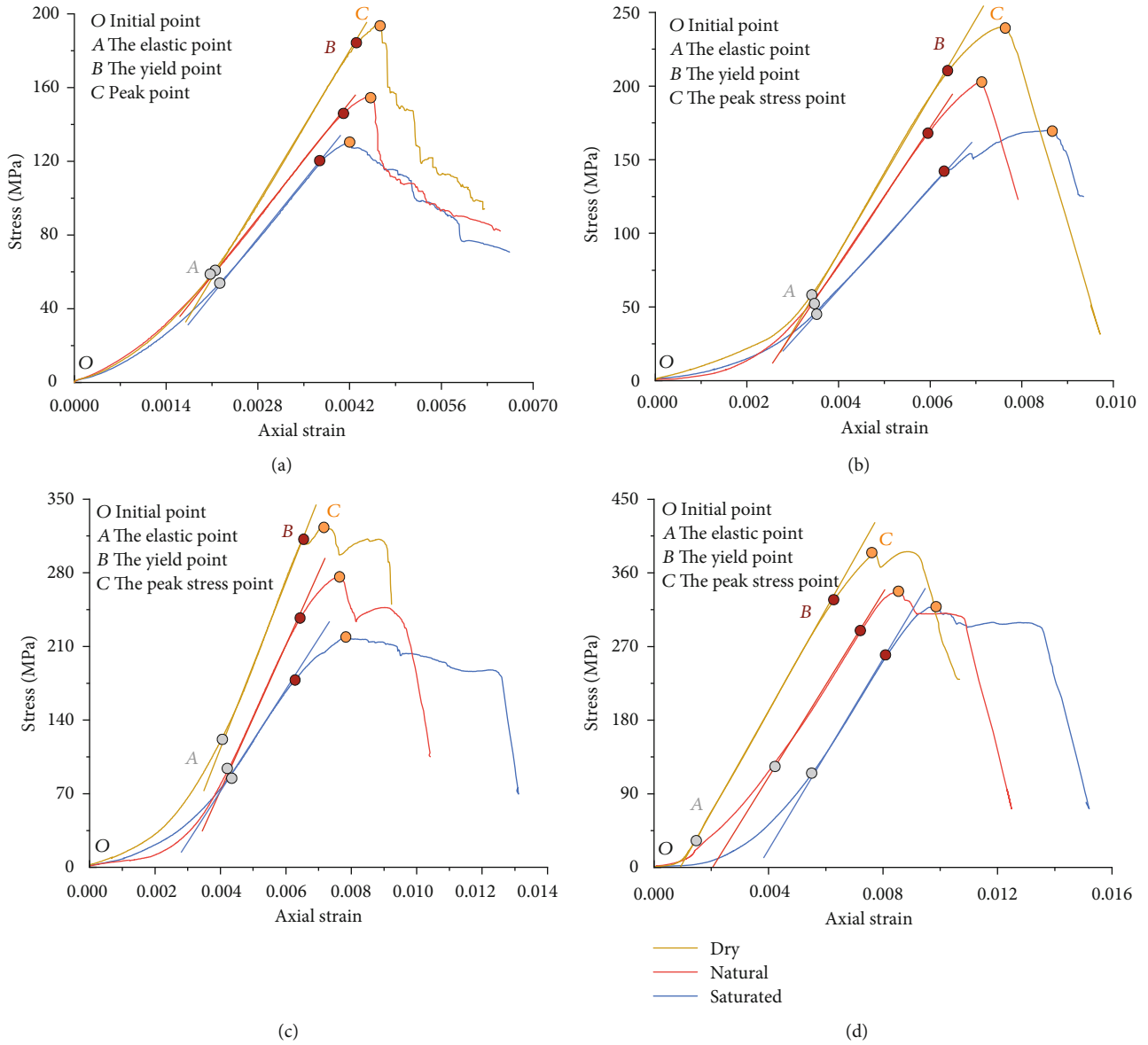


FIGURE 3: Stress-strain curves of granite samples with different water content under different confining pressure conditions: (a) $\sigma_3 = 0$ MPa (uniaxial compression); (b) $\sigma_3 = 5$ MPa; (c) $\sigma_3 = 10$ MPa; (d) $\sigma_3 = 20$ MPa.

increase of water content, the decrease rate of cohesion and internal friction angle of samples is relatively fast at lower water content (dry to natural state). In comparison, the decrease rate of cohesion and internal friction angle of samples is slow at higher water content (natural to saturated state), mainly because the water film has almost completely wrapped the mineral particles, and the lubricating softening and dissolving ability of water decreases.

4. Nonlinear Energy Evolution of Samples under Different Water Content States

4.1. Energy Analysis Principle of Rock Failure Process. The rock sample is deformed under the action of external force,

assuming that no heat exchange occurs with the outside world during the test process, that is, a closed system. The total input energy generated by the work of external force is U , which can be obtained according to the first law of thermodynamics [18]:

$$U = U^d + U^e, \quad (3)$$

where U^e is the elastic strain energy that the rock can release, this part of the energy is formed in the elastic strain stage of the rock mass unit. When the external force is removed, this part of the energy can restore the rock mass deformation to get some recovery. U^d is the dissipation energy of the rock used to form the internal damage and plastic deformation of the rock mass unit, and its change satisfies the second

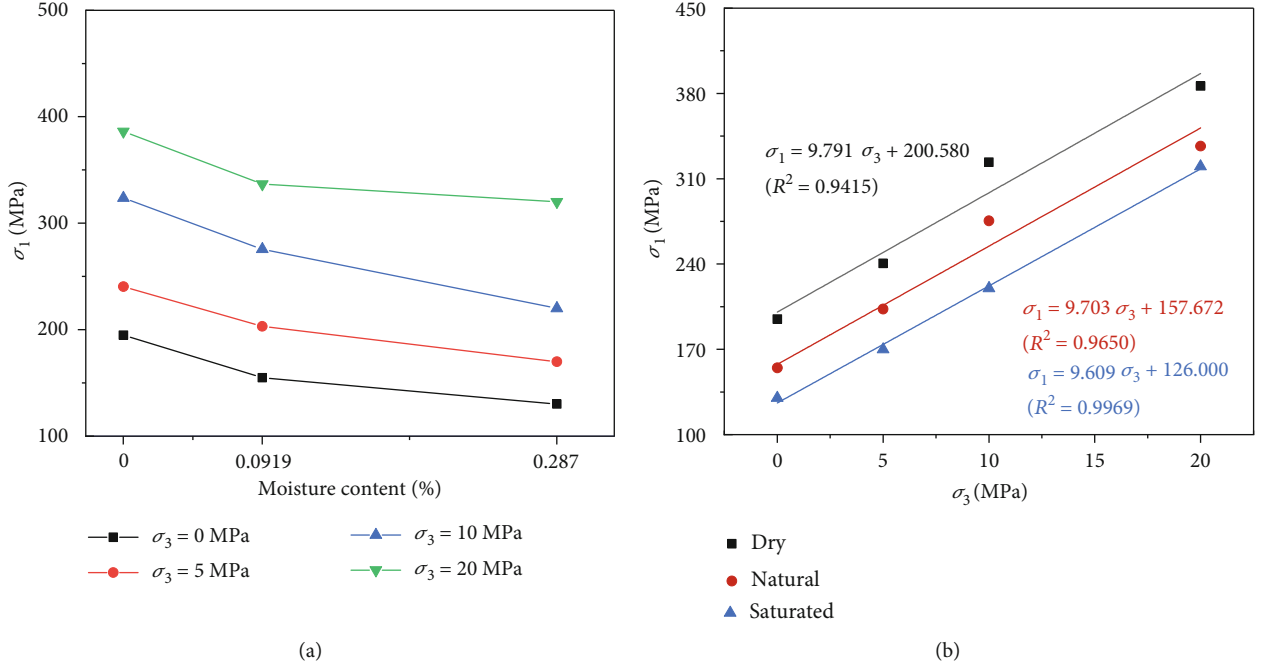


FIGURE 4: Strength change curve: (a) relationship between peak strength and water content; (b) relationship between peak strength and confining pressure.

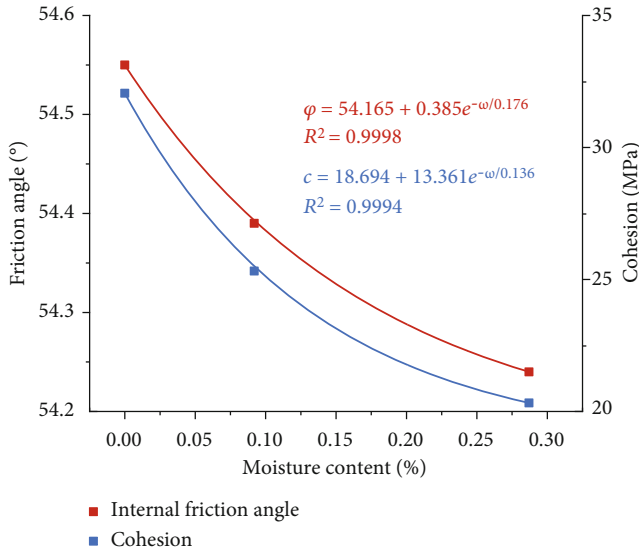


FIGURE 5: Relationship of cohesion and internal friction angle with water content.

law of thermodynamics. That is, the internal state change conforms to the trend of entropy increase.

Figure 6 shows the relationship between the dissipation energy and the elastic strain energy of the rock mass unit i during the deformation process [18]. The area U_i^d indicates the dissipation energy of the rock mass unit. The shaded area U_i^e means the strain energy stored in the rock mass unit and the elastic strain energy released after unloading the rock mass unit. E_i is unloading elastic modulus.

The energy of each part of the rock mass unit in the principal stress space can be expressed as [19]:

$$U = \int_0^{\varepsilon_1} \sigma_1 d\varepsilon_1 + \int_0^{\varepsilon_2} \sigma_2 d\varepsilon_2 + \int_0^{\varepsilon_3} \sigma_3 d\varepsilon_3, \quad (4)$$

$$U^e = \frac{1}{2} \sigma_1 \varepsilon_1^e + \frac{1}{2} \sigma_2 \varepsilon_2^e + \frac{1}{2} \sigma_3 \varepsilon_3^e, \quad (5)$$

$$\varepsilon_i^e = \frac{1}{E_i} [\sigma_i - \nu_i (\sigma_j + \sigma_k)], \quad (6)$$

where σ_i , σ_j , and σ_k ($i, j, k = 1, 2, 3$) are principal stresses. ε_i and ε_i^e are the strain and elastic strain in the principal stress direction, respectively. E_i and ν_i are the unloading elastic modulus and Poisson's ratio. For the convenience of calculation, the initial elastic modulus E_0 and Poisson's ratio ν can be used instead for numeration, and the elastic modulus and Poisson's ratio in the later elastic stage are taken [18].

Thus, the elastic strain energy U^e can be written as

$$U^e = \frac{1}{2E_0} [\sigma_1^2 + \sigma_2^2 + \sigma_3^2 - 2\nu(\sigma_1\sigma_2 + \sigma_2\sigma_3 + \sigma_1\sigma_3)]. \quad (7)$$

Under the uniaxial compression condition, $\sigma_2 = \sigma_3 = 0$, and substituting it into Equations (4) and (7), the energy of the rock under the uniaxial compression condition can be calculated as follows:

$$U = \int_0^{\varepsilon_1} \sigma_1 d\varepsilon_1, \quad (8)$$

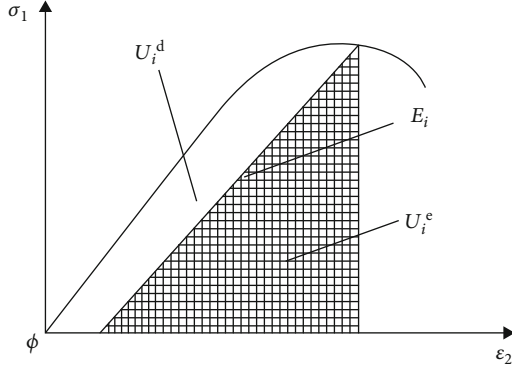


FIGURE 6: Relationship between dissipation energy U_i^d and releasable strain energy U_i^e in the rock unit.

$$U^e = \frac{1}{2E_0} \sigma_1^2. \quad (9)$$

Under conventional triaxial compression conditions, $\sigma_2 = \sigma_3$, and substituting it into Equations (4) and (7), the energy of the rock under conventional triaxial compression conditions can be calculated as follows:

$$U = \int_0^{\epsilon_1} \sigma_1 d\epsilon_1 + 2 \int_0^{\epsilon_3} \sigma_3 d\epsilon_3, \quad (10)$$

$$U^e = \frac{1}{2E_0} [\sigma_1^2 + 2\sigma_3^2 - 2\nu(\sigma_3^2 + 2\sigma_1\sigma_3)].$$

4.2. Energy Evolution Characteristics of Samples with the Different Water Content States. The laws of thermodynamics indicate that energy conversion is the intrinsic essence of changing the physical characteristics of matter [18]. Therefore, from the perspective of energy, the damage to failure of the sample is the evolution of a macroscopic instability phenomenon driven by energy. That results from the combined effect in the accumulation and transformation processes of the dissipation energy, elastic strain energy, etc. Based on Equations (4) and (9) to (11), the total input energy, elastic strain energy, and dissipation energy of granite samples in dry, natural, and saturated states under each confining pressure condition can be calculated. The relationship between the total input energy, elastic strain energy, dissipation energy, and axial strain of the three water content states under each confining pressure condition can be obtained, as shown in Figure 7.

As shown in Figure 7, the energy evolution trend of granite samples under different confining pressure and water content states is approximately the same. With the increasing axial strain of the sample, the total input energy of the sample continues to increase, the elastic strain energy first increases and then decreases, and the dissipation energy rises slowly in the early stage and starts to increase rapidly near the dilatancy point.

In the compaction stage (OA stage), the energy input by the testing machine is partly converted into dissipation energy required for the closure of the primary microcracks

in the sample and partially stored as elastic strain energy. From Figure 7, the dissipation and elastic strain energy curves almost coincide, and both energies are slowly increasing. In the elastic stage (AB stage), the total input energy of the sample continues to grow, and the curves of elastic strain energy and dissipation energy are gradually separated. After that, the total input energy and elastic strain energy increase rapidly, while the dissipation energy increases extremely slowly, indicating that almost all the energy input from outside at this stage is converted into elastic strain energy and stored in rock. In the plastic stage (BC stage), the percentage of total input energy conversion of the sample changes. The proportion of conversion into the dissipation energy increases, so the dissipation energy increases rapidly, the cracks inside the rock sample are produced in large numbers and expand continuously, and the damage of the sample gradually increases. The proportion of conversion into the elastic strain energy decreases, and the increased rate of elastic strain energy slows down until the peak point reaches the extreme value. At this time, the elastic strain energy stored in the sample is the rock energy storage limitation. In the failure stage (after point C), the elastic strain energy accumulated inside the sample is rapidly released, and the dissipation energy is increased quickly. Most of the external energy input is converted into dissipation energy and used for crack expansion, penetration, shear-slip deformation along the penetration surface, etc.

4.3. Water Content Effect of Energy Evolution. Due to the limitation space for this article, the water content effect of the total input energy, elastic strain energy, and dissipation energy evolution of granite samples under different water content states is analyzed in this paper by taking the test with the confining pressure of 0 MPa (uniaxial compression) as an example. The energy evolution characteristics of the three samples with different water content states are shown in Figure 8.

As Figure 8(a) shows, the total input energy of samples in different water content states versus the axial strain curve exhibits stage characteristics. It has experienced three stages: upward concave acceleration increase, nearly linear constant velocity increase, and downward concave deceleration increase, with an overall S-shape. With the rise in water content of samples, the total energy growth rate decreases, and the total input energy at the same axial strain is reduced.

As Figure 8(b) shows, in the compaction stage (OA stage), the elastic strain energy of samples in different water content states has little difference. In the elastic stage (AB stage), the increase rate in elastic strain energy of the three water content samples shows an apparent difference, the lower the water content, the faster the growth of elastic strain energy. In the plastic stage (BC stage), the increased rate of elastic strain energy of each water content sample shows a slowly decreasing trend. The higher the water content, the growth rate of elastic strain energy reduces significantly. When the peak axial strain is reached, the granite samples of each water content state get energy storage limitation, and the energy storage limitation of the samples in different water content states are significantly different.

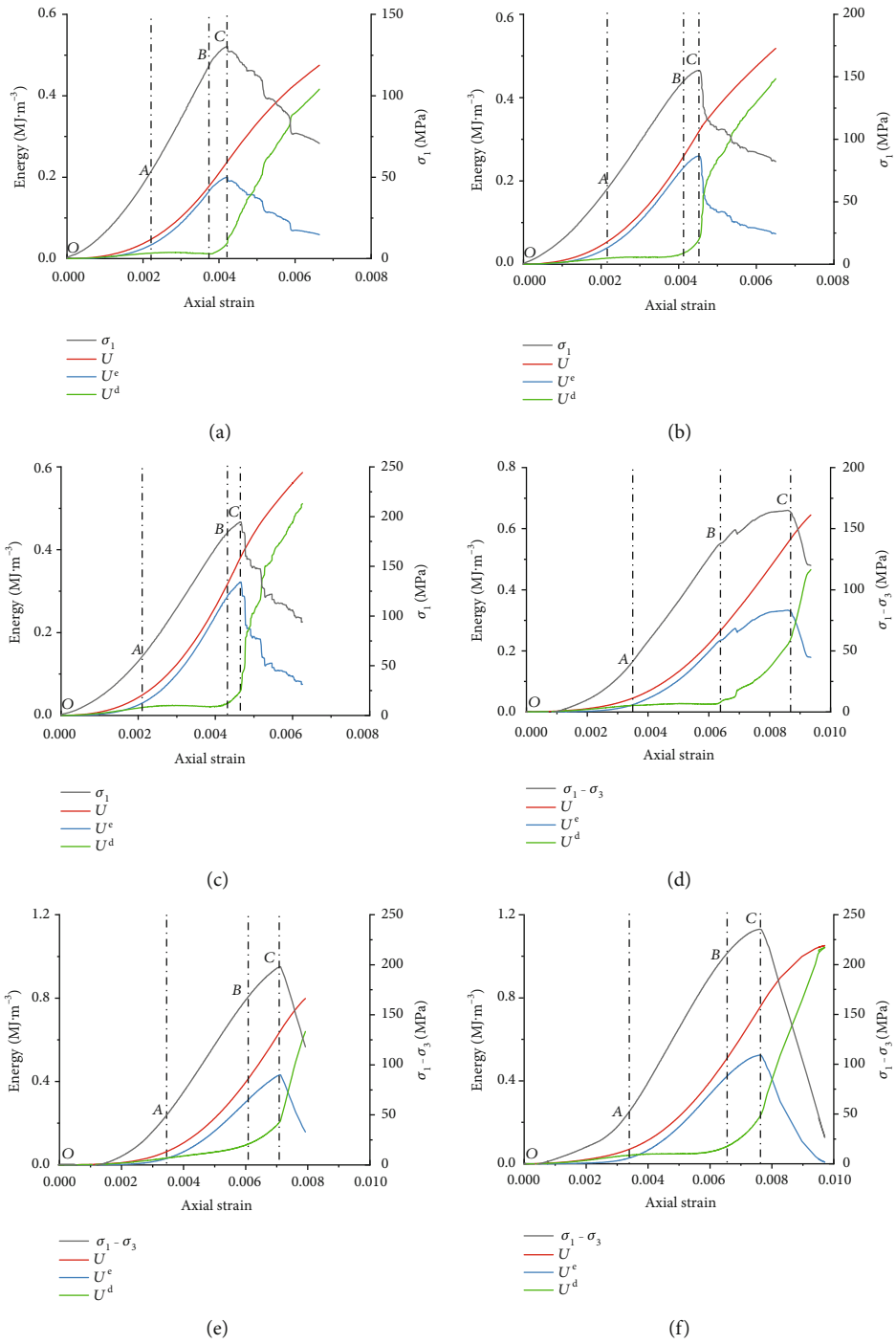


FIGURE 7: Continued.

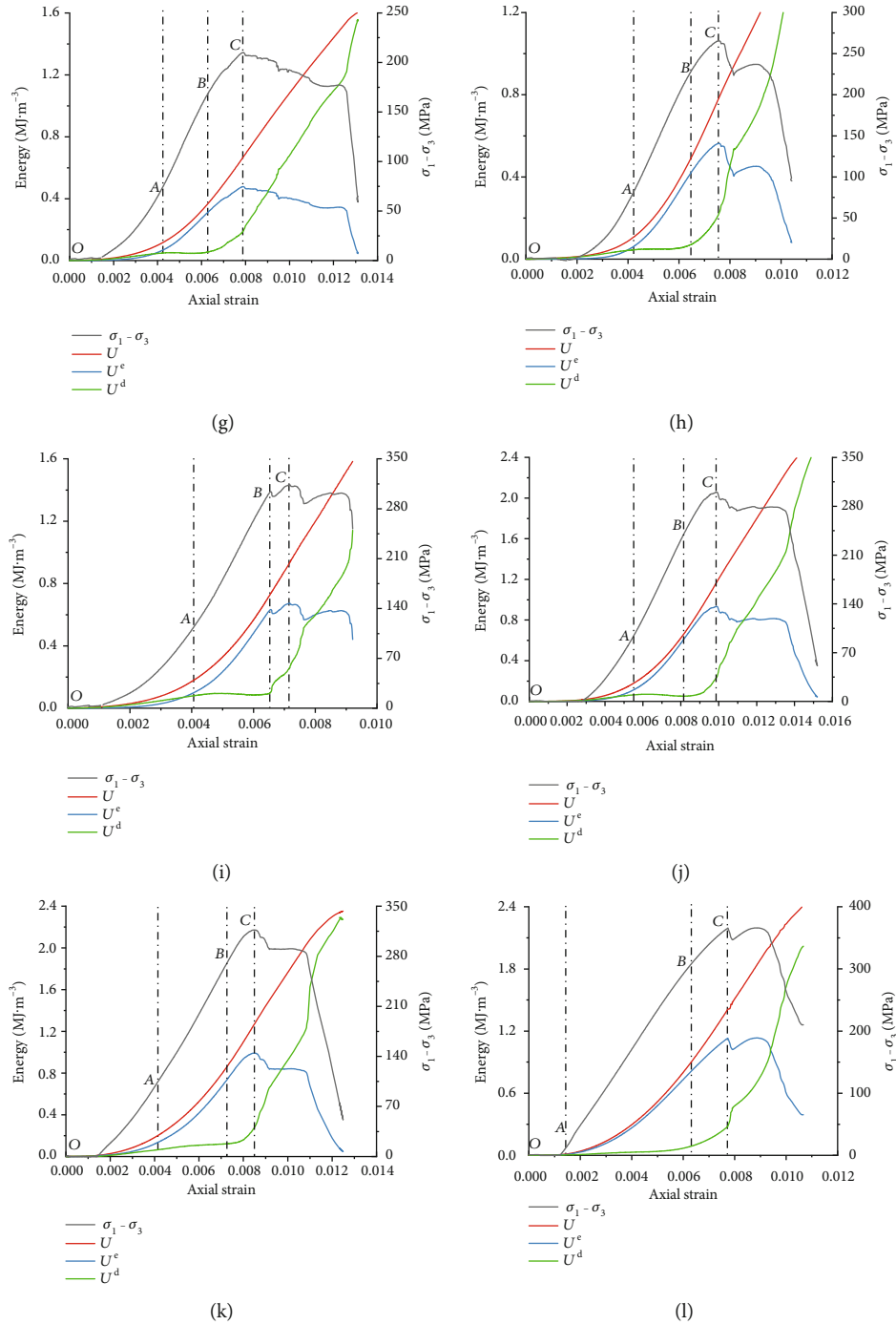


FIGURE 7: Energy evolution characteristics of granite samples under different conditions: (a) saturated state, $\sigma_3 = 0$ MPa; (b) natural state, $\sigma_3 = 0$ MPa; (c) dry state, $\sigma_3 = 0$ MPa; (d) saturated state, $\sigma_3 = 5$ MPa; (e) natural state, $\sigma_3 = 5$ MPa; (f) dry state, $\sigma_3 = 5$ MPa; (g) saturated state, $\sigma_3 = 10$ MPa; (h) natural state, $\sigma_3 = 10$ MPa; (i) dry state, $\sigma_3 = 10$ MPa; (j) saturated state, $\sigma_3 = 20$ MPa; (k) natural state, $\sigma_3 = 20$ MPa; (l) dry state, $\sigma_3 = 20$ MPa.

The higher the water content, the lower the energy storage limitation of the samples. The energy storage limitation of the sample in the dry state is 0.3220 MJ/m^3 , and in the natural state is 0.2593 MJ/m^3 , while the energy storage limitation in the saturated state is reduced to 0.1998 MJ/m^3 . In the failure stage (after point C), the elastic strain energy stored in the samples starts to release rapidly, and the water

content has a significant effect on the elastic strain energy release rate. The elastic strain release rate of the dry state sample is the largest, and the elastic strain energy and axial strain curves show a vertical drop. The elastic strain release rate of the natural state sample is the second, and the elastic strain energy-axial strain curve shows the characteristics of vertical drop followed by a gradual and slow decline. The

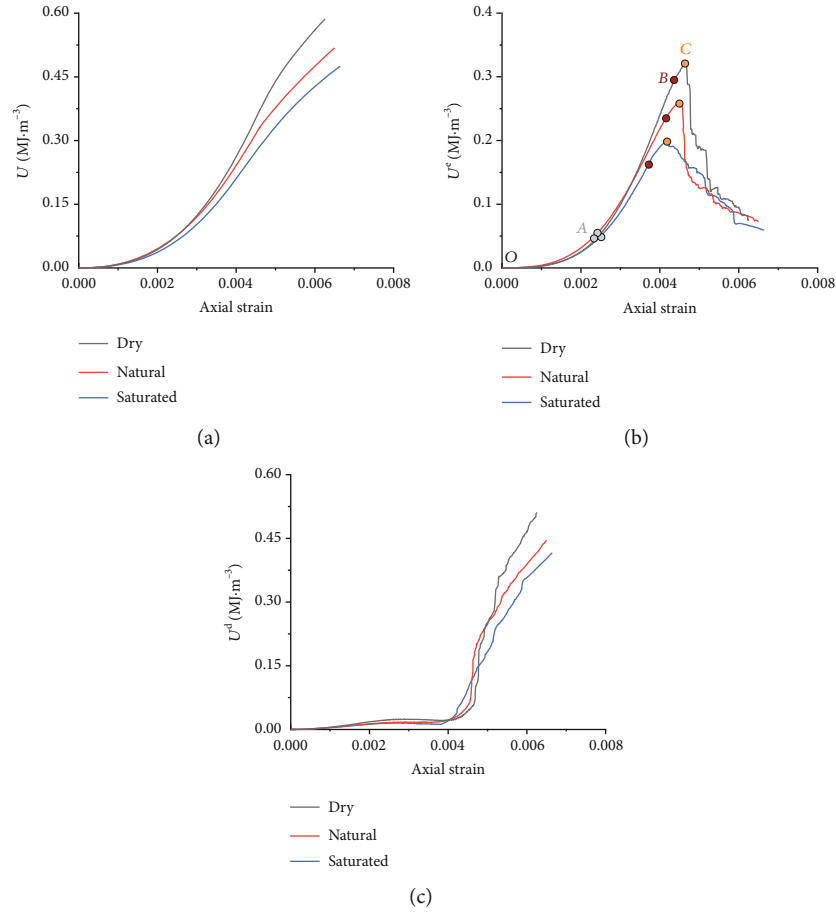


FIGURE 8: Energy evolution characteristics of granite samples with different water content states (confining pressure 0 MPa): (a) total input energy; (b) elastic strain energy; (c) dissipation energy.

elastic strain release rate of the saturated state sample is the slowest, and the elastic strain energy-axial strain curve does not show a vertical drop but a relatively slow decline.

Energy dissipation is the essential property of rock deformation and failure, and the process is unidirectional and irreversible. Part of the strain energy is dissipated in the form of plastic damage deformation energy and crack propagation fracture surface energy. Energy dissipation within the rock occurs in the links of the closing of primary cracks, the initiation and evolution of new microcracks, the formation of macrocracks, and plastic deformation. As Figure 8(c) shows, the dissipation energy increases slowly in the compaction and elastic stages, and the values are small. The effect of water content on the dissipation energy of the samples in these two stages is not apparent. In the plastic stage, the dissipation energy grows rapidly with the initiation, expansion, and penetration of cracks inside the samples. Since the water content has an important influence on the initiation, unstable extension, and connection of new cracks within the rock samples, the water content has a highly significant effect on the dissipation energy of the sample at this stage. The higher the water content, the greater the dissipation energy of the granite samples, and the earlier it starts to increase rapidly. When the sample deformation develops to the failure stage, the elastic strain energy is

released rapidly, and the dissipation energy increases abruptly. And it shows the characteristic that the lower the test water content, the faster the increase rate of the dissipation energy. The lower the water content of the samples when it is destroyed, the higher the final energy dissipated. Comparing Figures 8(b) and 8(c), the amount of energy dissipated by the samples with different water content states corresponds to the amount of elastic strain energy released by the samples after their peaks, considering the perspective of energy balance and transformation.

The total input energy and elastic strain energy at the peak point of the granite samples versus the water content are shown in Figures 9(a) and 9(b), respectively.

From Figure 9, water has a significant weakening effect on both total input energy and elastic strain energy at the peak point of granite samples. Take confining pressure 0 MPa for example: the total input energy of granite samples in the dry, natural, and saturated states are 0.446 MJ/m³, 0.320 MJ/m³, and 0.238 MJ/m³, respectively, and the total input energy of natural and saturated state is 71.749% and 53.363% of dry state, respectively. The elastic strain energy of granite samples in the dry, natural, and saturated states are 0.322 MJ/m³, 0.259 MJ/m³, and 0.198 MJ/m³, respectively, and the elastic strain energy of natural and saturated state is 80.435% and 61.491% of dry state, respectively. The

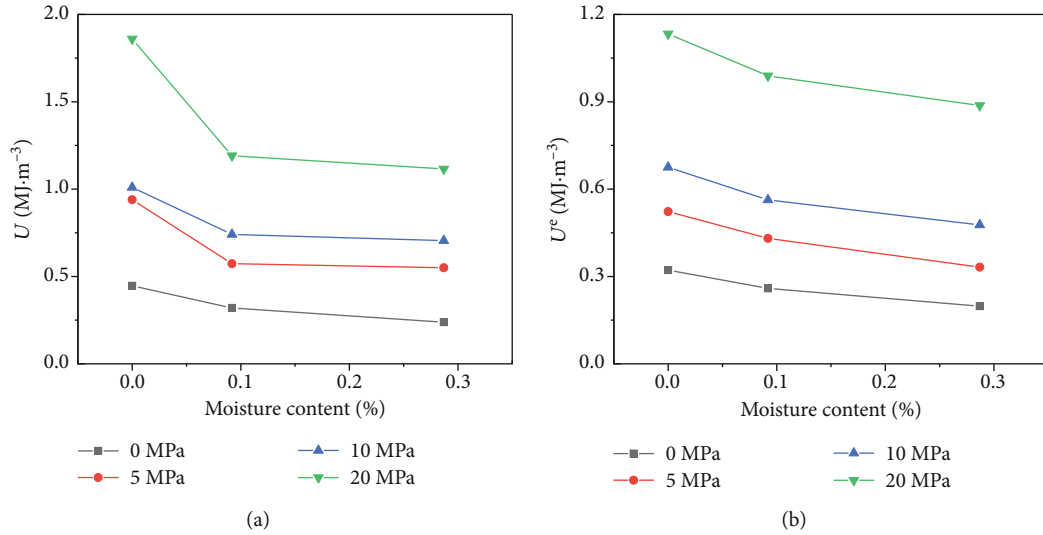


FIGURE 9: Relationship between the total input energy and elastic strain energy at peak point and water content: (a) total input energy; (b) elastic strain energy.

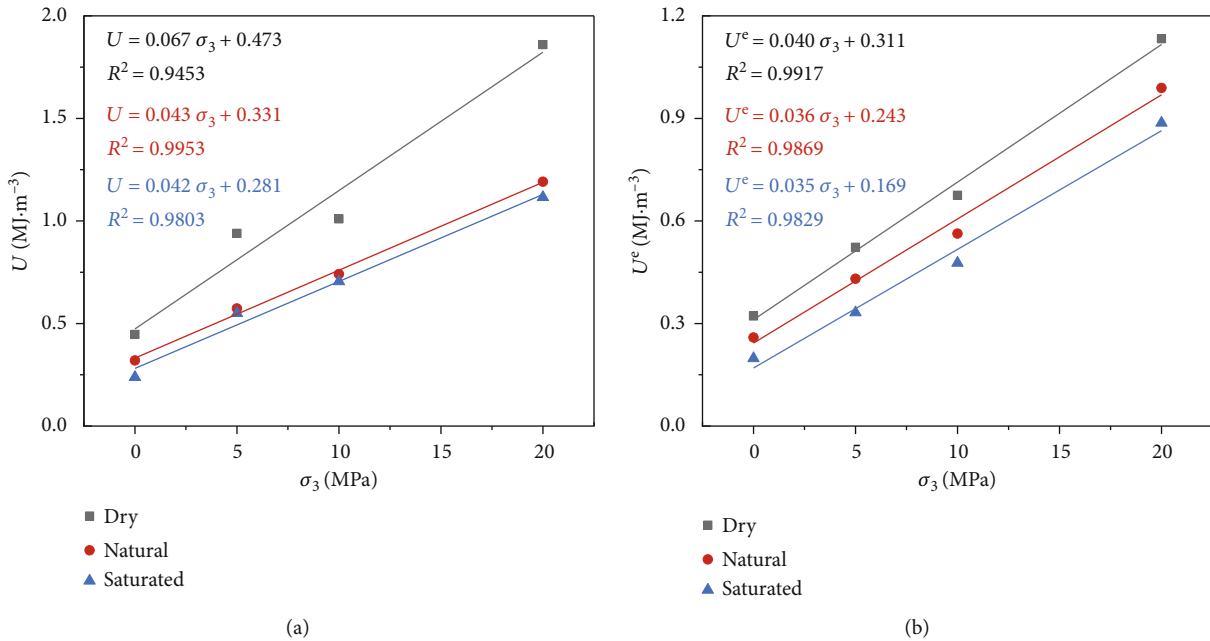


FIGURE 10: Relationship between the total input energy and elastic strain energy at peak point and confining pressure: (a) total input energy; (b) elastic strain energy.

total input energy and the elastic strain energy at the peak point have the same law of variation with the water content change but still differ. The total input energy decreases significantly at lower water content (dry to natural state), and the decline reduces at higher water content (natural to saturated state). The elastic strain energy decreases approximately linearly with the increase of water content.

The total input energy and elastic strain energy at the peak point of the granite samples versus the confining pressure are shown in Figures 10(a) and 10(b), respectively.

From Figure 10, the total input energy and elastic strain energy at the peak point of granite samples increase with the

increase of the confining pressure, and the two kinds of energy of the samples have an excellent linear relationship with the confining pressure. With the rise in water content, the slope of the fitting relationship between the total energy and elastic strain energy and the confining pressure decreases gradually, and the slope of the fitting relationship line of the total input energy is more affected by the increase in water content, indicating that the total energy of the samples is more affected by the water content, the water sensitivity is stronger. When the confining pressure increase is the same, the total input energy at the peak point and the stored elastic strain energy (energy storage limitation) of the granite

sample with higher water content are minor. Thus, the elastic strain energy released by the sample in the failure stage is less, and the ability of the sample to occur intense dynamic failure is reduced. This is the inherent reason for using rock injection to prevent impact pressure and rock burst in underground projects.

5. Nonlinear Models and Chaos Analysis of Energy Evolution

5.1. Nonlinear Evolution Model of Energy Evolution. Energy transformation is an essential feature of physical changes occurring in matter, and matter destruction is a state instability phenomenon driven by energy [20]. Energy exchange and transformation are constantly occurring during the deformation and destruction of rocks. The energy conversion of loaded rocks is driven by the strain hardening and strain softening mechanisms. The strain hardening mechanism converts the external input energy into strain energy of the rock. The strain softening mechanism converts the strain energy within the rock into other forms of energy, such as damage energy and heat energy, that is, the energy of higher quality into the energy of lower quality [21]. Strain hardening and strain softening mechanisms coexist throughout the whole deformation and failure process of rocks. The strain hardening mechanism is greater than the strain-softening mechanism in the prepeak stage, so the macroscopic presentation of strain hardening and energy accumulation. The latter is larger than the former in the postpeak stage, and the macroscopic performance is strain softening and energy release [20].

There are multiple microscopic mechanisms of hardening and softening within rocks, which have complex facilitating and constraining effects on each other. When an energy transformation process occurs, various microscopic mechanisms consume this energy. When one microscopic mechanism consumes energy and strengthens, the impact of other microscopic mechanisms is inhibited, and it is difficult to reach the equilibrium state, which will prevent the enhanced microscopic mechanism from consuming more energy and strengthening indefinitely. In addition, various micromechanisms also have a competitive relationship in the sample space. The more an energy microscopic mechanism consumes in a specific sample area, the more it restricts other microscopic mechanisms. Also, this microscopic mechanism is inhibited in other sample areas [22]. The interaction of microscopic mechanisms within the rock sample leads to a complex nonlinear rather than a simple linear relationship in the energy evolution mechanism of the sample.

Considering the complexity of multiple hardening and softening microscopic mechanisms and various nonlinear effects, mathematical equations can be developed to describe the transfer of energy during rock deformation [22]. However, it is challenging to implement and cannot be applied to quantitative analysis due to too many variables. For simplicity, only the action of external loads and the action of energy self-repression are considered. The nonlinear model of energy evolution in terms of the generalized rate of

change of energy transformations is more practical for the case of anthropogenic rock unloading (as opposed to natural geological processes such as earthquakes). At a certain level of deviator stress ($\sigma_1 - \sigma_3 = \Delta\sigma$), the generalized rate of change of elastic strain energy ($1/U^e \cdot dU^e/d\Delta\sigma$) is related to the total input energy U , the elastic strain energy U^e , and the minimum activation energy U^{e0} required to drive the activation of the energy accumulation mechanism, because the rock energy accumulation mechanism works only when the total input energy U reaches or exceeds the minimum activation energy U^{e0} [22–24]. The more U of the rock sample, the more favorable the activation of the energy accumulation mechanism. Thus, the generalized rate of change of elastic strain energy ($1/U^e \cdot dU^e/d\Delta\sigma$) is proportional to U , and because the sample energy accumulation mechanism works only when $U_0 - U^{e0} > 0$, thus the generalized rate of change of elastic strain energy ($1/U^e \cdot dU^e/d\Delta\sigma$) is proportional to $(U_0 - U^{e0})$, namely

$$\frac{1}{U^e} \frac{dU^e}{d\Delta\sigma} \propto (U_0 - U^{e0}). \quad (11)$$

When the energy accumulated in the rock sample increases and gradually reaches the energy storage limitation of the rock, the energy accumulation mechanism is prevented from working again. Therefore, the generalized rate of change of elastic strain energy ($1/U^e \cdot dU^e/d\Delta\sigma$) is proportional to the negative value of U^e , namely

$$\frac{1}{U^e} \frac{dU^e}{d\Delta\sigma} \propto (-U^e). \quad (12)$$

In summary, the mathematical model of the differential form of the energy evolution of the rock sample can be developed as shown in the following equation:

$$\frac{1}{U^e} \frac{dU^e}{d\Delta\sigma} = a(U_0 - U^{e0}) - bU^e, \quad (13)$$

where a and b are coefficients, reflecting the degree of energy accumulation and inhibition of the role of accumulation. For the same energy conversion process in the same loaded rock, a and b are constants, and different values are taken for different lithologies and energy conversion processes. Solving the differential equation shown in Equation (13) gives

$$U^e = \frac{k}{1 + e^{-r\Delta\sigma - kn}}, \quad (14)$$

where $k = a(U_0 - U^{e0})/b$, $r = a(U_0 - U^{e0}) = kb$, and n is the integration constants. The nonlinear evolution model of the total input energy and dissipation energy during rock deformation can be established according to a similar idea, and limited to the space of this article, only the nonlinear mathematical model of elastic strain energy evolution is given in this paper.

The test data of different samples are fitted according to Equation (14). The fitting curves and mathematical equations of the elastic strain energy of the three water content

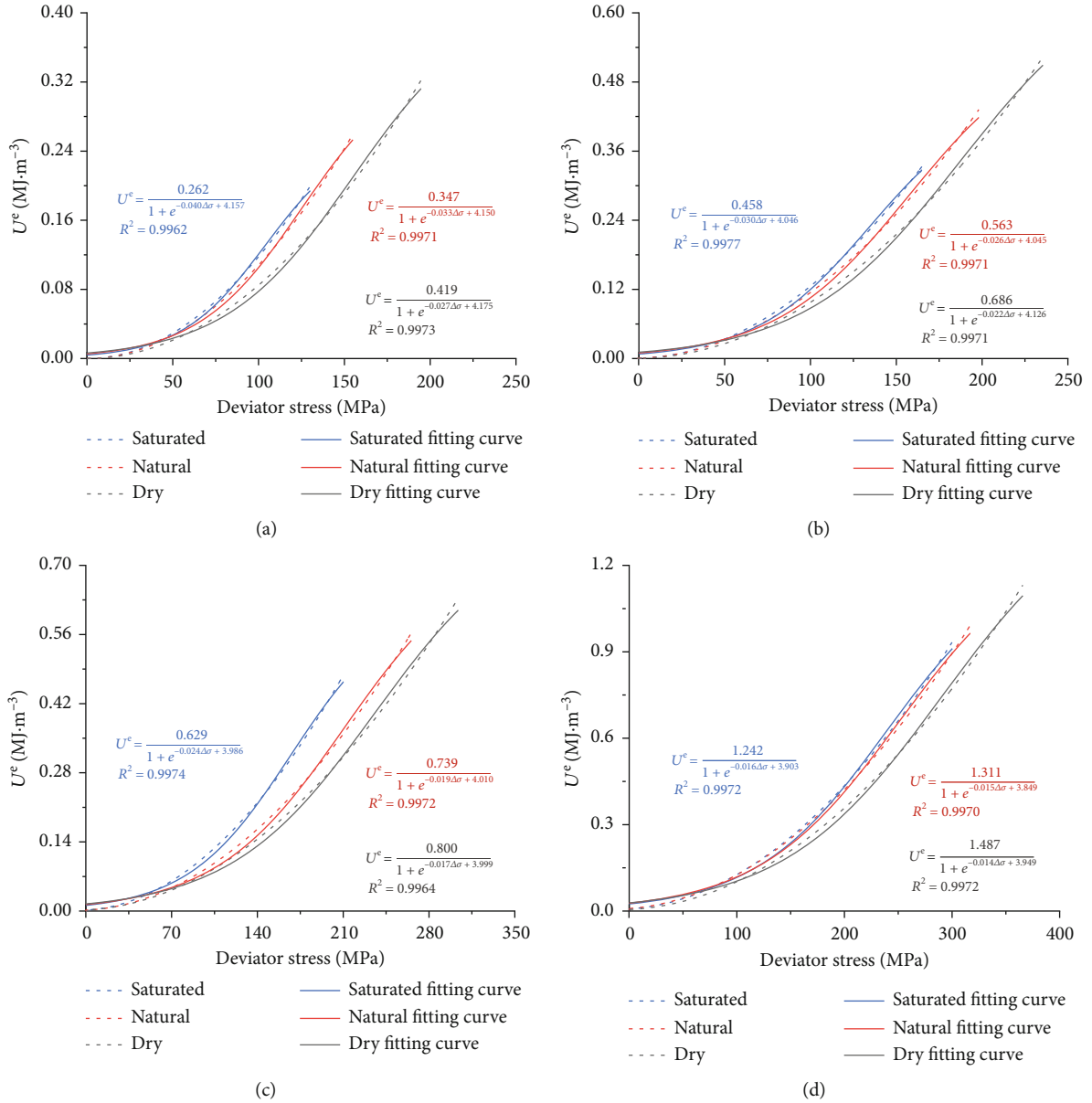


FIGURE 11: Relationship between U^e and deviator stress in granite with three water content states under different confining pressure and its nonlinear fitting equation: (a) $\sigma_3 = 0$ MPa; (b) $\sigma_3 = 5$ MPa; (c) $\sigma_3 = 10$ MPa; (d) $\sigma_3 = 20$ MPa.

state samples under different confining pressures can be obtained, as shown in Figure 11.

As shown in Figure 11, the fitting relation coefficients (R^2) of each fitted relationship curve are above 0.996, and the fitting accuracy of Equation (14) is very high. Indicating the established nonlinear evolution mathematical model can accurately describe the various characteristics and laws of elastic strain energy in the prepeak stages of deformation of granite samples at different confining pressure and water content conditions.

In the mathematical Equation (14) of the energy nonlinear evolution model, the parameter k represents the maximum value that the elastic strain energy U^e can theoretically reach. According to the fitting equation shown

in Figure 11, the variation law of parameter k with water content state and confining pressure can be obtained, as shown in Figure 12.

From Figure 12, the parameter k increases with the increase of the confining pressure and decreases with the rise in the water content. It shows that the theoretical maximum value of the elastic strain energy stored in the sample increases with the confining pressure and decreases with the increase of the water content. The variation characteristics based on the nonlinear energy model are consistent with the test results of the energy evolution law of the granite samples in the previous section. The theoretical maximum value of the elastic strain energy U^e of the sample expressed by the parameter k is different from the actual energy storage

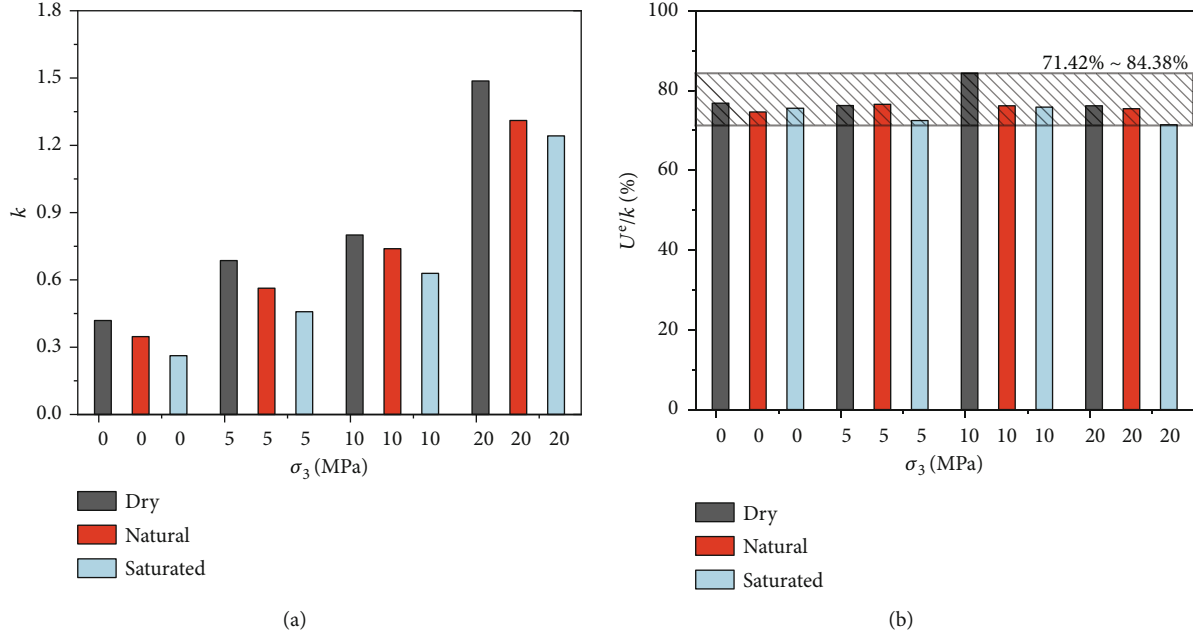


FIGURE 12: The variation law of parameter k value under different confining pressure and water content state and its relationship with the energy storage limitation: (a) energy fitting parameter k values; (b) relationship between parameter k value and energy storage limitation.

limitation shown in Figures 9 and 10. The real energy storage limitation of granite is only about 75-85% of the theoretical maximum value because the deviator stress ($\Delta\sigma$) cannot reach infinity in the actual test.

5.2. Chaos Analysis of Nonlinear Energy Evolution. Equation (14) is the classical generalized logistic equation. To further study the nonlinear characteristics of granite energy evolution and analyze the evolution sequence of energy with deviator stress, Equation (14) is rewritten as a discrete form of logistic model [25]:

$$U_{n+1}^e = \mu U_n^e \left(1 - \frac{U_n^e}{k} \right), \quad (15)$$

where U_n^e is the elastic strain energy density of the sample under a particular deviator stress level $\Delta\sigma_n$. U_{n+1}^e is the elastic strain energy of the sample at the deviator stress level $\Delta\sigma_{n+1} = \Delta\sigma_n + \Delta\sigma$. μ is the energy iterative growth factor, characterizing the iterative growth effect of rock energy during the loading process. k is the maximum value of U_n^e .

Let $U_n^e/k = \beta_n^e$, Equation (15) can be written in the form of a standard logistic equation with chaotic properties:

$$\beta_{n+1}^e = \mu \beta_n^e (1 - \beta_n^e), \quad (16)$$

where $\beta_n^e \in [0, 1]$, $\beta_{n+1}^e \in [0, 1]$, and $\mu \in [0, 4]$. Equation (16) shows that the energy evolution process of the loaded rock can be represented by the standard logistics equation with chaotic properties. The energy evolution of the rock loading process has bifurcation and chaotic characteristics.

Relevant studies have shown that different energy iterative growth factor μ values make β_n^e sequences exhibit dif-

ferent orbits [24]. When $\mu < 1.0000$, the iteration result $\beta_n^e = 0$ is the only stable state, which means that there is no elastic strain energy accumulated in the system, and the system has been in a stable condition. However, with the external energy input during the loading process, materials such as rocks are bound to accumulate elastic strain energy, so the interval $\mu < 1.0000$ cannot exist in practice. When $1.0000 \leq \mu < 3.0000$, the energy increases continuously with the increase of the value of μ , and its stable state is the equilibrium point $\beta_n^e = 1 - 1/\mu$ after the contraction of the phase space. When the value of μ increases to the critical point of 3.0000, the original equilibrium point becomes unstable and enters the period-doubling bifurcation area, and a series of bifurcation points appear, and with the increase of μ , the bifurcation process accelerates. When μ increases to the critical value of 3.5699, the multiply-periodic bifurcation process ends, and the rock system enters the chaos area. The relationship between the energy iterative growth factor μ and the deviator stress under different confining pressure conditions is shown in Figure 13.

It can be seen from Figure 13 that the changing trend of the μ value of the three water content states granite samples under different confining pressure conditions is the same. It increases monotonically with the increase of deviator stress. The μ value increases relatively slowly at the initial loading stage and then increases rapidly. The μ value of the granite sample is significantly affected by the water content. Under the same deviator stress case, the μ value of the saturated state samples is larger than that of the natural state samples, and the μ value of the natural state samples is larger than that of the value of the dry state samples. The greater the water content of the granite samples, the greater the increase rate of its μ value. The granite sample system with high

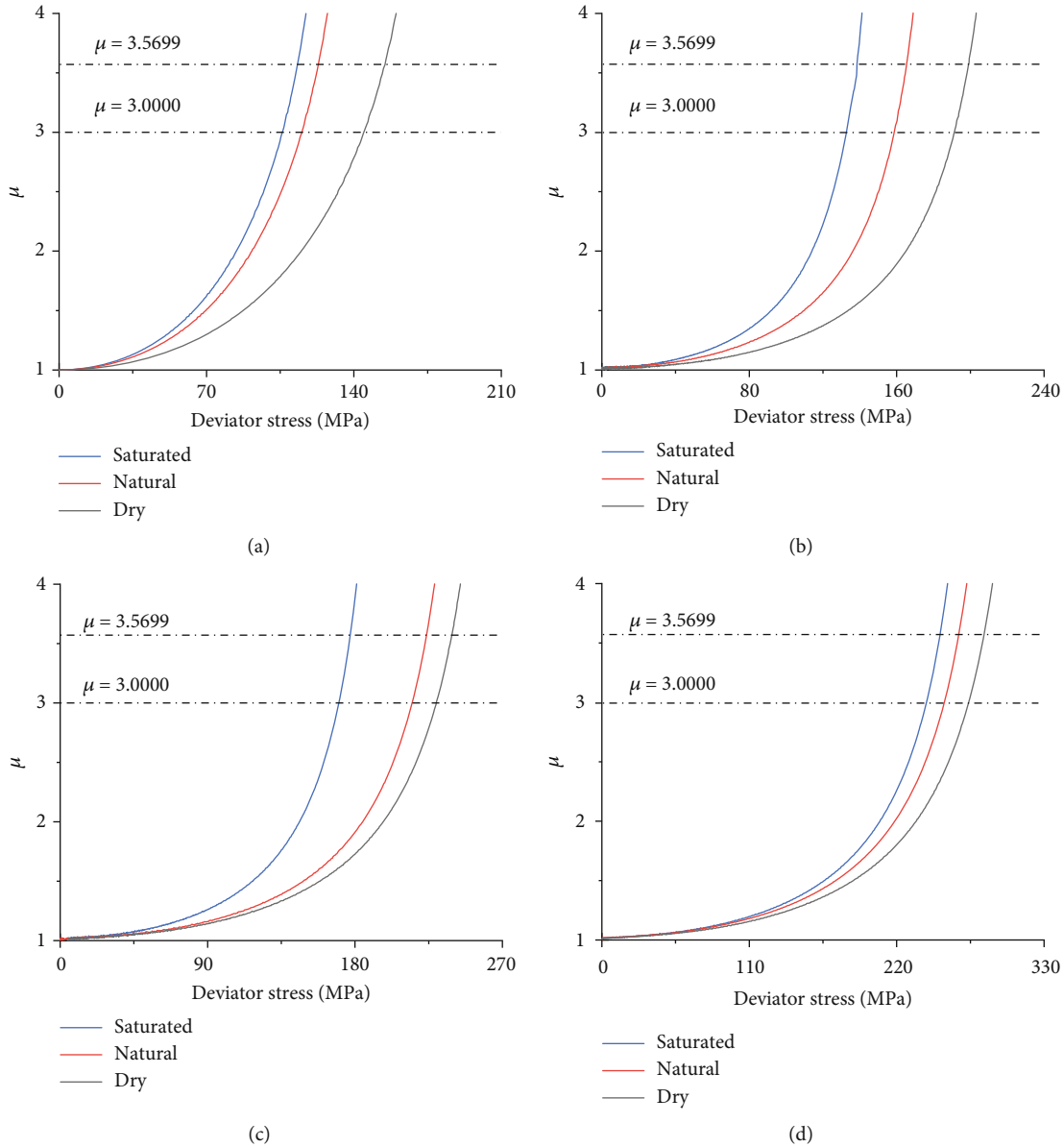


FIGURE 13: Evolution curve of μ value with deviator stress under different confining pressure and water content state: (a) $\sigma_3 = 0$ MPa; (b) $\sigma_3 = 5$ MPa; (c) $\sigma_3 = 10$ MPa; (d) $\sigma_3 = 20$ MPa.

water content develops from the stable area to the period-doubling bifurcation area and chaos area at a smaller deviator stress level.

In the process of increasing the deviator stress on granite samples, the μ value and the elastic strain of samples also increase. The elastic strain energy accumulated and stored inside the samples rises, the energy accumulation density increases, and its stable state is the equilibrium point $\beta_n^e = 1 - 1/\mu$ after the phase space contraction. When the deviator stress of the granite samples in the three water content states under different confining pressure conditions increases to 73.28%-81.71% of the peak deviator stress of samples (see Figure 14(a)), the μ value increases to the critical value of 3.0000. The ratio of the elastic strain energy to the peak elastic strain energy is 55.36%~67.29% (see Figure 14(a)), the

equilibrium point is unstable, and the granite sample systems start to enter the period-doubling bifurcation area. When the deviator stress of the granite samples increases to 76.22%~86.86% of the peak deviator stress of samples (see Figure 14(b)), the μ value rises to the critical value of 3.5699. The ratio of the elastic strain energy to the peak elastic strain energy is 62.04%~75.83% (see Figure 14(b)), the period-doubling bifurcation area ends, and the granite sample systems start to enter the chaos area.

It can be seen from Figure 14 that when the granite sample enters the period-doubling bifurcation area ($\mu = 3.0000$) and the chaos area ($\mu = 3.5699$), the proportion of deviator stress and elastic strain energy of the sample increased slightly overall with the increase of the water content of the sample.

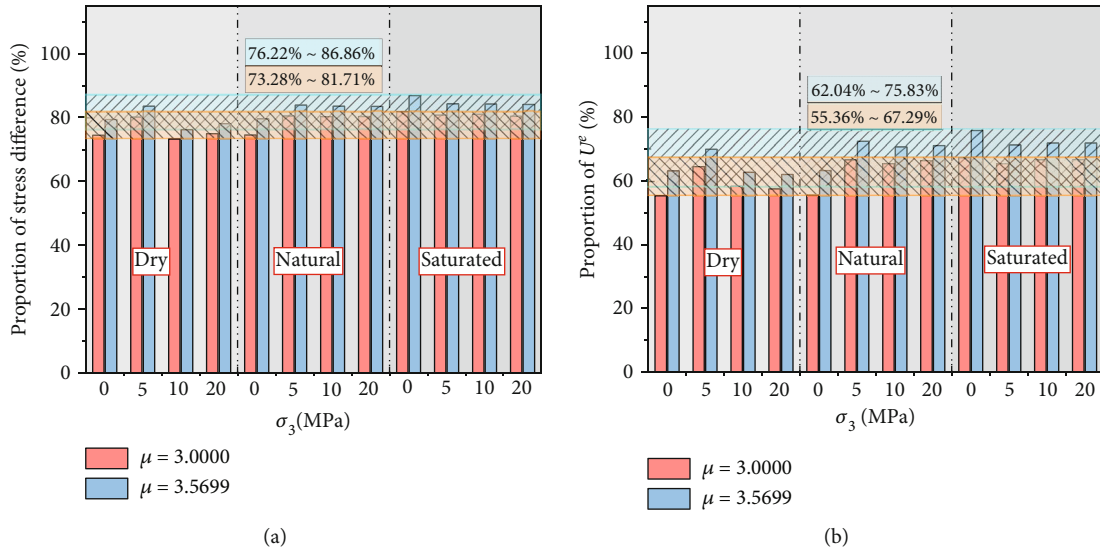


FIGURE 14: Proportion of deviator stress and elastic strain energy corresponding to different μ values: (a) proportion of deviator stress; (b) proportion of elastic strain energy.

6. Failure Mode of Granite Sample and Its Relationship with Energy

It can be seen from the above that the mechanical properties and energy evolution characteristics of granite samples under different confining pressure conditions change significantly with the change in water content. Thus, this inevitably leads to a different failure morphology of granite samples after loading under different confining pressure and water content conditions. The failure morphology of granite samples under different test conditions was collected by images in this test, as shown in Table 1.

As can be seen from Table 1

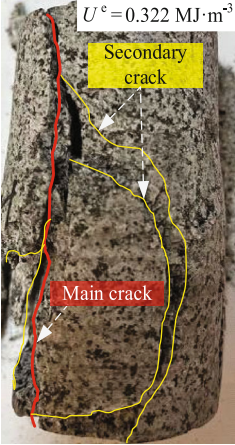
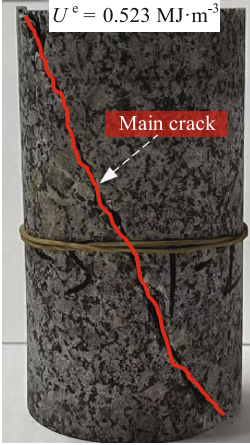
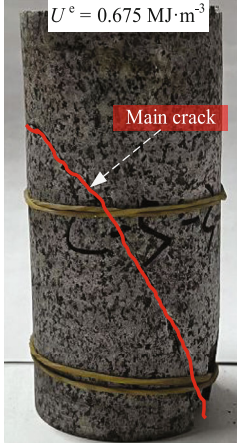
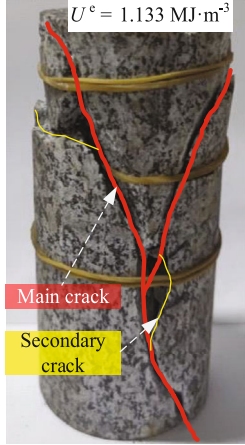
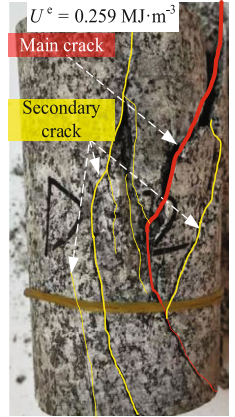
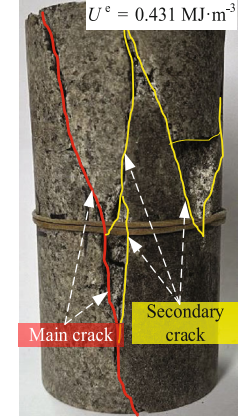
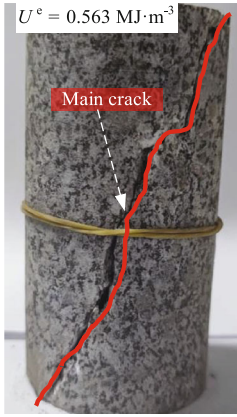

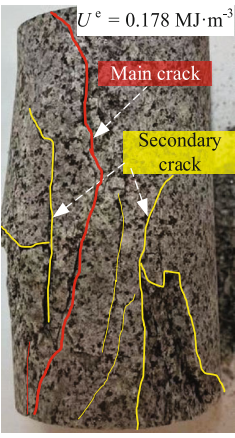
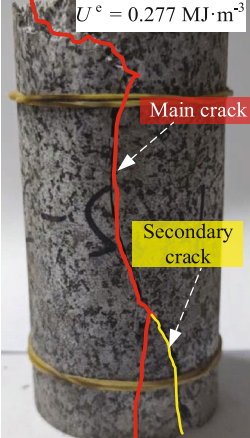
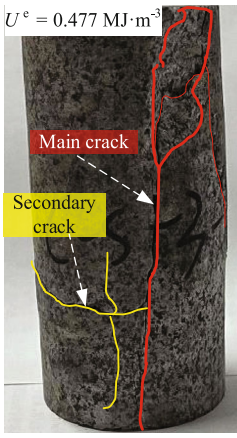

- (1) the failure characteristics of granite samples under different confining pressure and water content are other. The samples in this test mainly show three modes of failure: splitting failure, splitting-shear composite failure, and shear failure. The failure modes of granite samples are jointly influenced and controlled by the two conditions of water content and confining pressure
- (2) for the dry state granite samples, splitting failure occurs only when the confining pressure is 0 MPa, and shear failure (including single failure surface shear failure and conjugated shear failure) occurs under other confining pressure conditions. For the natural state granite samples, splitting failure occurs when the confining pressure is 0 MPa, splitting-shear composite failure occurs when the enclosing pressure is 5 MPa, and single failure surface shear failure occurs when the confining pressure is 10 MPa and 20 MPa. For the saturated state granite samples, splitting failure occurs when the confining pressure is 0 MPa and 5 MPa, splitting-shear composite failure occurs when the confining pressure is 10 MPa,

and single failure surface shear failure occurs when the confining pressure is 20 MPa

- (3) due to the limitation of the confining pressure on the extension and penetration of the longitudinal tensile crack, the failure modes of granite samples gradually change from splitting failure, splitting-shear composite failure to single failure surface shear failure, and conjugated shear failure with the increase of the confining pressure under the same water content of the same sample
- (4) with the increase of water content (from the dry state to the saturated state), under the condition of low confining pressure (0 MPa), the failure mode of the granite sample changes from the splitting failure of the main tension crack accompanied by the local compression shear crack to the splitting failure of multiple longitudinal tension cracks. Under moderate confining pressures (5 MPa and 10 MPa), the failure mode changes from the shear failure to splitting failure or split-shear composite failure. When the confining pressure is higher (20 MPa), the failure mode changes from the conjugated shear failure to the single failure plane shear failure

The whole process of rock deformation and failure is accompanied by the processes of energy input, energy accumulation, energy dissipation, and energy release. The external force works on the loaded and deformed rock, which causes external energy input into the loaded rock. Part of the input energy is converted into elastic strain energy and accumulated in the rock. In contrast, the other part is dissipated in plastic deformation energy, damage energy, etc. The increasing accumulation of elastic strain energy increases the driving force of rock failure, and the energy dissipation caused by the nonlinear properties inside the rock lowers the threshold of rock failure. Therefore, one (elastic strain

TABLE 1: Failure morphology of granite under different conditions.

Moisture states	Confining pressure					
	0 MPa	5 MPa	10 MPa	20 MPa		
Dry	 <p>$U^e = 0.322 \text{ MJ}\cdot\text{m}^{-3}$</p> <p>Secondary crack</p> <p>Main crack</p> <p>Splitting failure</p>	 <p>$U^e = 0.523 \text{ MJ}\cdot\text{m}^{-3}$</p> <p>Main crack</p> <p>Single failure plane shear failure</p>	 <p>$U^e = 0.675 \text{ MJ}\cdot\text{m}^{-3}$</p> <p>Main crack</p> <p>Single failure plane shear failure</p>	 <p>$U^e = 1.133 \text{ MJ}\cdot\text{m}^{-3}$</p> <p>Main crack</p> <p>Secondary crack</p> <p>Conjugated shear failure</p>		
	Natural	 <p>$U^e = 0.259 \text{ MJ}\cdot\text{m}^{-3}$</p> <p>Main crack</p> <p>Secondary crack</p> <p>Splitting failure</p>	 <p>$U^e = 0.431 \text{ MJ}\cdot\text{m}^{-3}$</p> <p>Main crack</p> <p>Secondary crack</p> <p>Splitting-shear composite failure</p>	 <p>$U^e = 0.563 \text{ MJ}\cdot\text{m}^{-3}$</p> <p>Main crack</p> <p>Single failure plane shear failure</p>	 <p>$U^e = 0.989 \text{ MJ}\cdot\text{m}^{-3}$</p> <p>Main crack</p> <p>Single failure plane shear failure</p>	
		Saturated	 <p>$U^e = 0.178 \text{ MJ}\cdot\text{m}^{-3}$</p> <p>Main crack</p> <p>Secondary crack</p> <p>Splitting failure</p>	 <p>$U^e = 0.277 \text{ MJ}\cdot\text{m}^{-3}$</p> <p>Main crack</p> <p>Secondary crack</p> <p>Splitting failure</p>	 <p>$U^e = 0.477 \text{ MJ}\cdot\text{m}^{-3}$</p> <p>Main crack</p> <p>Secondary crack</p> <p>Splitting-shear composite failure</p>	 <p>$U^e = 0.887 \text{ MJ}\cdot\text{m}^{-3}$</p> <p>Main crack</p> <p>Single failure plane shear failure</p>

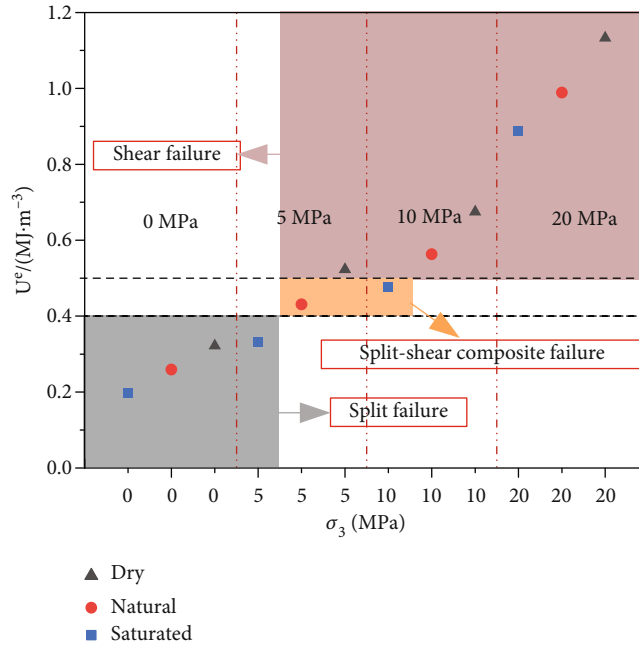


FIGURE 15: Relationship between rock failure modes and energy storage limitation.

energy) makes the rock more destructive, and the other (dissipation energy) causes the rock to be less resistant to failure. When the elastic strain energy is stored to a specific limitation and exceeds the extreme value that the constantly damaged rock can load, the rock is fractured and destabilized and releases the elastic strain energy to the outside world. From the above energy-driven nature of rock failure, the differences in energy accumulation, dissipation, and release characteristics of the three water content granite samples under different confining pressures must lead to differences in the failure modes, as shown in Table 1. The higher the elastic strain accumulated in the prepeak stage of granite samples, the greater the energy released during the instability failure of the sample. So more fracture surfaces formed by the expansion and penetration of high-energy compressive shear cracks need to be generated to provide a release path. From the analysis in Section 4.3, the higher the confining pressure and the lower the water content, the higher the elastic strain energy accumulated in the prepeak stage of the granite sample. Therefore, the saturated state samples under high confining pressure or the natural and dry state samples under moderate and high confining pressure exhibit shear failure caused by the expansion and penetration of high energy compressive shear cracks. In contrast, splitting failure occurs in low confining pressure samples or saturated state samples under moderate confining pressure caused by the expansion and penetration of tension cracks of two orders of magnitude from energy-consuming horizontal low-pressure shear cracks [26]. The rest of the granite samples, under the intermediate conditions, occurs the transitional failure of the two below failure modes: splitting-shear composite failure.

The energy storage limitation of the rock is the maximum elastic strain energy that can be accumulated and loaded by the sample that continuously dissipates energy and gradually increases the degree of damage. Essentially,

it results from the evolution and game between the elastic strain energy and dissipation energy in the prepeak stage. The rock energy storage limitation is the energy state that corresponds to the critical failure state of the rock. The higher the rock energy storage limitation, the greater the energy released in the postpeak instability stage of the rock, and the energy release characteristics are directly related to the final macroscopic failure morphology of the sample, so the rock energy storage limitation must be intrinsically linked to its failure mode. The relationship between the failure mode of granite samples and the energy storage limitation of the samples under different confining pressure and water content states in this test is shown in Figure 15.

From Figure 15, the granite failure mode in this test has a good matching relationship with the distribution range of energy storage limitation of the sample. Therefore, although the water content state and confining pressure conditions can affect the failure mode of the rock, the energy mechanism behind both is the fundamental reason for determining the macroscopic failure mode of the rock. Combined with Table 1, for the granite samples with splitting failure, the distribution of energy storage limitation ranges from 0.198 MJ/m³ to 0.322 MJ/m³. For the samples whose final failure mode is the splitting-shear composite failure, the energy storage limit ranges from 0.431 MJ/m³ to 0.477 MJ/m³. The granite samples whose energy storage limitation is between 0.523 MJ/m³ and 1.133 MJ/m³ exhibit shear failure. According to the limited energy storage limitation data of this paper, the energy storage limitation of 0.40 MJ/m³ and 0.50 MJ/m³ can be taken as the energy limit value of the failure mode transformation of granite samples for this test initially, and the final or more accurate energy limit value is subject to further in-depth and systematic study.

7. Conclusions

- (1) Under the condition of low confining pressure and low water content, the whole stress-strain curve of granite shows a stress drop after the peak, while under the condition of high confining pressure or high water content, it shows partial ductility characteristics. And the ductility failure characteristic of granite is more evident with the increase in water content and confining pressure. With the increase of water content, the compressive strength of granite samples decreases significantly, and the water content weakens the confining pressure effect of compressive strength. The cohesion and internal friction angle of granite show a nonlinear decrease with the increase of water content, and the reduction of cohesion is more significant
- (2) The energy evolution trend of granite samples under the three water content states is roughly the same. The total input energy has experienced three stages of upward concave slow increase, nearly linear constant velocity increase, and downward concave deceleration increase. The higher the water content, the less the total input energy of the granite sample. The elastic strain energy increases first and then decreases. The higher the water content, the slower the elastic strain energy rises, the lower the energy storage limitation, and the lower the postpeak release rate. The dissipation energy increases slowly in the early stage and then increases rapidly. The higher the water content, the earlier the dissipation energy rises significantly, but the final dissipation energy is lower when the sample is destroyed
- (3) Considering the self-inhibition effect of energy, a nonlinear model of energy evolution of granite is established from the perspective of the generalized change rate of energy conversion, and the nonlinear mathematical equation of energy-deviator stress evolution is obtained. The verification shows that the equation can accurately describe the various characteristics of the elastic strain energy at the prepeak stage of granite under different confining pressure and water content. The higher the water content of the granite, the greater the energy iterative growth factor and its increasing rate. Meanwhile, the granite system can enter period-doubling bifurcation and chaos areas at a relatively lower level of deviator stress, and the proportion of deviator stress and elastic strain energy is larger during state transitions
- (4) The failure modes of granite are jointly influenced and controlled by the two conditions of water content and confining pressure, showing three modes: splitting failure, splitting-shear composite failure, and shear failure. The saturated state samples under high confining pressure or natural and dry state samples under moderate and high confining pressure exhibit shear failure. And the splitting failure

occurs in the samples of low confining pressure or moderate confining pressure with saturated state samples. Under intermediate conditions, the rest of the samples undergo the transitional type of splitting-shear composite failure. The failure mode of granite has a good matching relationship with the distribution range of energy storage limitation

Data Availability

The data used to support the findings of this study are available from the corresponding author upon request.

Conflicts of Interest

The authors declare no conflict of interest.

Acknowledgments

This research was funded by the National Natural Science Foundation of China (Grant Nos. 52178388, 51778215, and U1810203) and China Postdoctoral Science Foundation Funded Project (Grant No. 2018M631114).

References

- [1] S. She and L. Dong, "Statistics and analysis of academic publications for development of rock mechanics in China," *Chinese Journal of Rock Mechanics and Engineering*, vol. 32, no. 3, pp. 442–464, 2013.
- [2] Z. Q. Zhou, L. P. Li, S. S. Shi et al., "Study on tunnel water inrush mechanism and simulation of seepage failure process," *Rock and Soil Mechanics*, vol. 41, no. 11, pp. 3621–3631, 2020.
- [3] K. H. Holmøy and B. Nilsen, "Significance of geological parameters for predicting water inflow in hard rock tunnels," *Rock Mechanics and Rock Engineering*, vol. 47, no. 3, pp. 853–868, 2014.
- [4] F. He, *The Research on Mechanism of Rock Creep-Seepage Coupling*, Liaoning Technical University, Fuxin, 2010.
- [5] B. Yang, *Spatio-Temporal Variation of Fractures in Overburden Due to Mining and Risk Assessment Model for Water and Sand Inrush*, China University of Mining and Technology, Xuzhou, 2018.
- [6] J. Guo, X. Liu, and C. Qiao, "Experimental study of mechanical properties and energy mechanism of karst limestone under natural and saturated states," *Chinese Journal of Rock Mechanics and Engineering*, vol. 33, no. 2, pp. 296–308, 2014.
- [7] L. I. Tian-bin, C. H. E. N. Zi-quan, C. H. E. N. Guo-qing, M. Chun-chi, T. Ou-ling, and W. Min-jie, "An experimental study of energy mechanism of sandstone with different moisture contents," *Rock and Soil Mechanics*, vol. 36, no. S2, pp. 229–236, 2015.
- [8] G. Chen, T. Li, W. Wang, Z. Zhu, Z. Chen, and O. Tang, "Weakening effects of the presence of water on the brittleness of hard sandstone," *Bulletin of Engineering Geology and the Environment*, vol. 78, pp. 1471–1483, 2017.
- [9] Z. Chen, C. He, D. Wu, G. Xu, and W. Yang, "Fracture evolution and energy mechanism of deep-buried carbonaceous slate," *Acta Geotechnica*, vol. 12, no. 6, pp. 1243–1260, 2017.
- [10] S. Wang, Y. Zhao, Z. Zou, and H. Jia, "Experimental research on energy release characteristics of water-bearing sandstone

- alongshore wharf,” *Pol Marit Res*, vol. 24, no. S2, pp. 147–153, 2017.
- [11] Y. Zhao, T. Yang, T. Xu, P. Zhang, and W. Shi, “Mechanical and energy release characteristics of different water-bearing sandstones under uniaxial compression,” *International Journal of Damage Mechanics*, vol. 27, pp. 640–656, 2018.
- [12] J. D. Jiang, S. S. Chen, J. Xu, and Q. S. Liu, “Mechanical properties and energy characteristics of mudstone under different containing moisture states,” *Journal of China Coal Society*, vol. 43, no. 8, pp. 2217–2224, 2017.
- [13] J. Geng and L. Cao, “Failure analysis of water-bearing sandstone using acoustic emission and energy dissipation,” *Engineering Fracture Mechanics*, vol. 231, article 107021, 2020.
- [14] X. P. Lai, S. Zhang, F. Cui, Z. Wang, H. Xu, and X. Fang, “Energy release law during the damage evolution of water-bearing coal and rock and pick-up of AE signals of key pregnancy disasters,” *Chinese Journal of Rock Mechanics and Engineering*, vol. 39, no. 3, pp. 433–444.
- [15] C. Li, N. Liu, W. Liu, and R. Feng, “Study on characteristics of energy storage and acoustic emission of rock under different moisture content,” *Sustainability*, vol. 13, p. 1041, 2021.
- [16] H. Ma, Y. Song, S. Chen et al., “Experimental investigation on the mechanical behavior and damage evolution mechanism of water-immersed gypsum rock,” *Rock Mechanics and Rock Engineering*, vol. 54, no. 9, pp. 4929–4948, 2021.
- [17] C. E. Fairhurst and J. A. Hudson, “Draft ISRM suggested method for the complete stress-strain curve for intact rock in uniaxial compression,” *International Journal of Rock Mechanics and Mining Science and Geomechanics Abstracts*, vol. 36, no. 3, pp. 281–289, 1999.
- [18] H. Xie, Y. Ju, and L. Li, “Criteria for strength and structural failure of rocks based on energy dissipation and energy release principles,” *Chinese Journal of Rock Mechanics and Engineering*, vol. 24, no. 17, pp. 3003–3010, 2005.
- [19] R. Solecki and R. J. Conant, *Advanced Mechanics of Materials*, Oxford University Press, London, 2003.
- [20] Z. Zhao and H. Xie, “Energy transfer and energy dissipation in rock deformation and fracture,” *Journal of Sichuan University*, vol. 40, no. 2, pp. 26–31, 2008.
- [21] R. Li, *Nonequilibrium thermodynamics and dissipative structures*, Tsinghua University Press, Beijing, 1986.
- [22] Z. Zheng, “Energy transfer process in rock deformation and rock deformation dynamics analysis,” *Scientia Sinica Chimica*, vol. 20, no. 5, pp. 524–537, 1990.
- [23] L. Zhang, Y. Cong, F. Meng, Z. Wang, P. Zhang, and S. Gao, “Energy evolution analysis and failure criteria for rock under different stress paths,” *Acta Geotechnica*, vol. 46, pp. 569–580, 2020.
- [24] Z. Zhang and F. Gao, “Research on nonlinear characteristics of rock energy evolution under uniaxial compression,” *Chinese Journal of Rock Mechanics and Engineering*, vol. 31, no. 6, pp. 1198–1207, 2012.
- [25] A. Yu, *A Study on Logistic Model*, Nanjing Forestry University, Nanjing, 2003.
- [26] X. Chen and Q. Zhang, “Research on the energy dissipation and release in the process of rock shear failure,” *Journal of Mining & Safety Engineering*, vol. 27, no. 2, pp. 179–184, 2010.